Effect of bismuth iodide (BiI 3) interfacial layer with different HTL's in FAPI based perovskite solar cell – SCAPS – 1D study

S. Karthick, Johann Bouclé, S. Velumani

Version of Record: https://www.sciencedirect.com/science/article/pii/S0038092X21001559
Manuscript_6292370469571507dce5d07b1383b2b2

Effect of Bismuth iodide (BiI_3) interfacial layer with different HTL's in FAPI based perovskite solar cell – SCAPS - 1D study

S. Karthick [a, b], J. Bouclé [b, *], S. Velumani [a, c, *]

(a) Programa de Nanociencias y Nanotecnología, Centro de Investigación y de Estudios Avanzados del Instituto Politécnico Nacional (CINVESTAV-IPN), Av. Instituto Politécnico Nacional 2508, Col. SanPedro Zacatenco, Ciudad de México, México, Código Postal 07360.

(b) Univ. Limoges, CNRS, XLIM, UMR 7252, F-87000 Limoges, France.

(c) Department of Electrical Engineering (SEES) Centro de Investigación y de Estudios Avanzados del Instituto Politécnico Nacional (CINVESTAV-IPN), Av. Instituto Politécnico Nacional 2508, Col. SanPedro Zacatenco, Ciudad de México, México, Código Postal 07360.

Abstract

In this paper, we numerically investigated the effect of Bismuth iodide (BiI_3) interfacial layer with different hole transport layer (HTL) candidates (including $Spiro-OMeTAD, Cu_2O, CuI, CuAlO_2, CuSbS_2, SrCu_2O_2, CuSCN, PTAA, P3HT$) in $FAPI$ based perovskite (i.e., $FA_{0.85}Cs_{0.15}Pb(I_{0.85}Br_{0.15})_3$) solar cells using Solar cell simulator capacitance software (SCAPS-1D). Our results reveal that the addition of a thin BiI_3 layer at the interface between the Perovskite active layer and the HTL efficiently improves hole extraction by defect passivation (i. e., reducing charge recombination and ion migration), which in turn enhances device performance compared to a typical reference architecture. The final optimized device photovoltaic parameters with interfacial layer confirm that the Cu-based HTL's, especially Cu_2O ($PCE = 24.07\,\%$), and $SrCu_2O_2$ ($PCE = 23.91\,\%$) HTL's are more suitable for the $FA_{0.85}Cs_{0.15}Pb(I_{0.85}Br_{0.15})_3$ solar cells than other HTL alternatives, including $Spiro-OMeTAD$ due to higher hole mobility and the valence-band offset alignment between Perovskite/HTL interface. Also, the influence of several metal electrodes (Ag, Cr, Cu, Au, Ni, Pt) is carefully studied with and without the BiI_3 interlayer. It is demonstrated that the energy band misalignment between the HTL and the metallic top electrode restricts charge collection, which is directly associated with low work functions. As a consequence, high work function electrodes such as $Au, Ni,$ and Pt have to be preferred in the presence or absence of the interlayer. The last section addresses the influence of the active layer, BiI_3 interlayer thicknesses on device performance and also the effect of parasitic resistances (R_{series} and R_{shunt}) were studied. From this analysis, BiI_3 interfacial layer seems highly beneficial for improving the performance of experimental perovskite solar cells.

Keywords: Bismuth iodide, interfacial layer, perovskite solar cells, SCAPS-1D, HTL.

1. Introduction

Due to the rapid improvement in the power conversion efficiency (PCE - up to 25.2 %) of organic-inorganic perovskite solar cells, it gains more attention from the photovoltaic community **(NREL, 2020).** The intrinsic instability and the presence of lead content in the formamidinium lead iodide ($FAPI$) perovskites, it forced researchers to develop stabilization (such as cation/halide engineering) and substitution strategies using various elements such as Sn, Bi, and Cu, etc. **(Lu et al., 2020).** Notably, organic cesium (Cs^+) cation and bromide (Br^-) halide mixed $FAPI$ perovskite absorber layer (i.e., $FA_{1-x}Cs_xPb(I_{1-x}Br_x)_3$) shown the remarkable and stable device performance than others because of their slow recombination rate as well as high charge carrier mobility behavior **(Groeneveld et al., 2020; McMeekin et al., 2016; Prathapani et al., 2018).** Mainly, $FA_{1-x}Cs_xPb(I_{1-x}Br_x)_3$ combination provides stability enhancement against the moisture and oxygen. Also, it is easier to alter the bandgap value (1.6 – 2 eV) while playing with halide ratio's (iodide and bromide) **(Nazarenko et al., 2017; Rehman et al., 2017; Sutter-Fella et al., 2018).** These perovskites are more suitable for tandem configurations. Recently, silicon-perovskite based tandem solar cells achieved an excellent efficiency of up to 29 % **(Bush et al., 2017; Eperon et al., 2016; Forgács et al., 2017; Köhnen et al., 2019; Lang et al., 2020; NREL, 2020; Zheng et al., 2018).**

For efficient photogeneration of electron (e^-) and hole (h^+) extraction from the perovskite layer and choosing the appropriate e^- and h^+ transport layer (ETL & HTL) is vital to enhance the PCE. Besides, the interfacial layer (IL) in between the perovskite absorber layer and the HTL interface is considered as a productive layer to avoid the immediate degradation of the absorber layer from external H_2O & O_2. Additionally, it helps to reduce the recombination at interfaces to improve the whole device's performance **(S. Wu et al., 2019).** In general, 64 % of the total solar model cost is related to the HTL (49 %) and the electrode (15 %), the blocking/interlayer cost approximately 0.6% only (Qiu et al., 2019). Besides the price, the organic HTL/electrode (Au or Ag) models suffers from the migration (i.e., metal ions from the metal electrode and halide ions from the perovskite absorber). Usually, there are four possible options to place the interfacial layers based on the planar conventional (n-i-p) and inverted (p-i-n) perovskite structures. Such as in the FTO/ETL interface, ETL/perovskite interface, perovskite/HTL interface, and HTL/electrode interface **(Cho and Park, 2017).** According to the previous reports, using additional IL in between the perovskite absorber layer and the HTL interface significantly enhances solar cell performance **(Cho and Park, 2017; Gharibzadeh et al., 2019; Gil-Escrig et al., 2015; Lee et al., 2014; Y. Liu et al., 2019; Noel et al., 2014; Song et al., 2016).** For example, N. K. Noel *et al.* introduced the thiophene and pyridine-based IL between perovskite/HTL interface and demonstrated that the IL improved the device efficiency from 13 % (without IL) to 15.3 % (with thiophene IL) and 16.5 % (with pyridine IL). Because of the passivation strategy, which significantly diminishes the nonradiative recombination pathways **(Noel et al., 2014).** D. Song *et al.* used the F4TCNQ IL and also achieved an enhanced efficiency from 15 % (without IL) to 18 % (with IL) because of the improved electric field, which mainly decreased the carrier loss at the surface and subsurface of the absorber layer. Also, IL creates an

energy barrier for the photogenerated e^- which reduces the recombination adjacent to Perovskite/HTL interface **(Song et al., 2016).** Some research groups used the halide perovskite layer as an IL; for example, J. W. Lee *et al.* deposited the thin $MAPbI_3$ layer over the $FAPbI_3$ absorber layer, they got the efficiency enhancement from 15.5% (without IL) to 16 % (with IL) due to an considerable increment in the conduction band minimum at the interface, leading to higher open-circuit voltage **(Lee et al., 2014).** Similarly, K. T. Cho *et al.* achieved an increased PCE from 18.9 % (without IL) to 21.3 % (with IL) using additional $FAPbBr_{3-x}I_x$ layer over the $(FAPbI_3)_{0.85}(MAPbBr_3)_{0.15}$ perovskite absorber, which efficiently suppresses the interfacial charge recombinations **(Cho et al., 2017).** In this perspective, using bismuth (Bi) based IL in perovskite device will be beneficial for the device performance. For example, L. Fu *et al.* employed the bismuth telluride (Bi_2Te_3) IL in HTL/Inorganic-Perovskite interface, and achieved an improved device performance from 7.4 % (without) to 11.9 % (with IL). These results clearly explain that, IL efficiently blocks the iodide ions migrations from the absorber layer **(Fu et al., 2019).** Also, bismuth iodide (BiI_3) material gains more attention due to its non-toxic behavior, a narrow bandgap (1.72 eV), a high absorption coefficient, and short carrier lifetimes, considering these properties of BiI_3, it is more suitable for photovoltaic applications **(Brandt et al., 2015a; Coutinho et al., 2019; Hamdeh et al., 2016; Hu et al., 2020; Lee et al., 2018; Yoo et al., 2019).** Moreover, according to the U. S. national mineral information center report, the Bismuth price is relatively too low compared to the lead (National Minerals Information Center, n.d.). Recently, Y. Hu *et al.* deposited the pristine BiI_3 IL over the titanium oxide ETL (i.e., ETL/Perovskite interface), and found that it improves the electron transport behavior by passivating the interfacial trap states. As a result, they got an increased PCE from 13.8 % (without) to 17.8 % (with IL) **(Hu et al., 2020).** But still, there is no BiI_3 IL-based simulation/theoretical analysis reported so far in the Perovskite/HTL interface.

Therefore, in this context, we theoretically introduce a thin BiI_3 IL between $FA_{0.85}Cs_{0.15}Pb(I_{0.85}Br_{0.15})_3$ absorber/Spiro-OMeTAD (HTL) layer using solar cell simulator capacitance software (SCAPS-1D) to understand the beneficial effect of BiI_3 on the device performance. Firstly, we construct an ideal n-i-p planar device without using the IL layer as a reference, and after placing a thin BiI_3 IL, our simulated device (FTO/ETL/Perovskite/BiI_3/HTL/Electrode) showed enhanced performance compared to the referenced one. Secondly, we carefully investigated the device performance using different HTL candidates, such as 2,2',7,7'-Tetrakis[N, N-di(4-methoxyphenyl)amino]-9,9'-spirobifluorene ($Spiro-OMeTAD$), cuprous oxide (Cu_2O), Strontium Cuprate ($SrCu_2O_2$), Cuprous Aluminate ($CuAlO_2$), copper antimony sulfide ($CuSbS_2$), cupric thiocyanate ($CuSCN$), Cuprous iodide (CuI), Poly(triarylamine) ($PTAA$), poly(3-hexylthiophene-2,5-diyl) ($P3HT$) with and without BiI_3 IL. The final optimized device photovoltaic parameters with IL confirms that the Cu-based Cu_2O, and $SrCu_2O_2$ HTL's are more suitable than other HTL nominees due to their band alignment with BiI_3 IL. Furthermore, we evaluated the effect of several electrodes (Ag, Cr, Cu, Au, Ni, Pt) based on their work function (WF) value with the above mentioned HTL's. At last, we studied the influence of IL thickness over the perovskite layer thickness and the effect of parasitic resistances (R_{series} and R_{shunt}) with suitable HTL. Our results deliver insightful facts to understand the effect of IL over the planar n-i-p $FAPI$ based perovskite device

structure, which is useful to enhance the PCE. As a result, using BiI_3 IL in between the perovskite/HTL interface could help to improve the experimental device performance.

2. Ideal device simulation methodology

Our simulated n-i-p device composed of FTO (transparent conductive oxide)/ SnO_2 (ETL)/ $FA_{0.85}Cs_{0.15}Pb(I_{0.85}Br_{0.15})_3$ (perovskite absorber layer)/BiI_3 (with and without - IL)/$Spiro-OMeTAD$ (HTL) /Au (electrode), shown in **Fig. 1**. In this study, all the simulations were carried out using solar cell simulator capacitance software (SCAPS-1D, version 3.3.07) to solve the Poisson and continuity equations **(Burgelman et al., 2000).** The simulated device was illuminated under one sun AM 1.5 G (100 mW cm^{-2}) solar spectrum with 300 k temperature, and the parasitic resistances (R_{Series} and R_{Shunt}) are not taken into these initial simulations. After illumination (photons strike) from ETL to HTL side (see **Fig.1**), the perovskite layer creates charge carriers, and diffuse into the electron (e^-) and hole (h^+) transport layers. Finally, $e^{-\prime}s$ and $h^{+\prime}s$ were collected by desired electrodes. The optimized absorber layer (500 nm), ETL (70 nm), all the HTL (150 nm), and IL (30 nm) thicknesses, as well as all other parameters such as e^- and h^+ mobility, e^- affinity, permittivity, the effective density of states, doping densities, and defect densities, are taken from previously published experimental and theoretical results, listed in Table I. **(Abdelaziz et al., 2020; Azri et al., 2019; Brandt et al., 2015b; Coulibaly et al., 2019; Coutinho et al., 2019; Han et al., 2014; Lee et al., 2018; Lin et al., 2020; Prathapani et al., 2018; Shasti and Mortezaali, 2019)** The employed e^- and h^+ velocity values are considered as $1 \times 10^7\ cm/s$. The work function of TCO (front contact - FTO) and electrode (back contact – Au) are set to 4.4 eV and 5.1 eV, respectively. All the simulation was done, without considering the optical reflectance of each layers at the interface nor surface. Simulating ideal devices is a first step to emphasize the influence of the IL on device operation, independently of the main electrical losses that are found in realistic devices. It is designed to help the experimentalist to tailor their experiments **(Karthick et al., 2020).** The effect of parasitic resistances (R_{Series} & R_{Shunt}) were demonstrated at the end of this paper. The energy band alignment between the absorber layer, ETL, IL, and all HTL illustrated in **Fig. 2**.

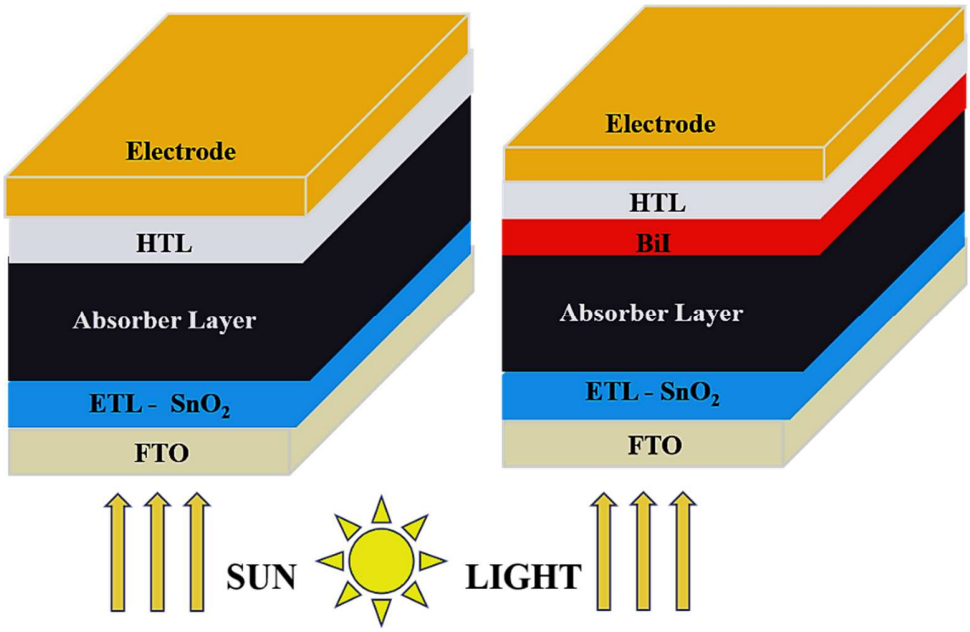

Fig. 1 The n-i-p typical perovskite solar cell structure (left) and with BiI_3 IL (right).

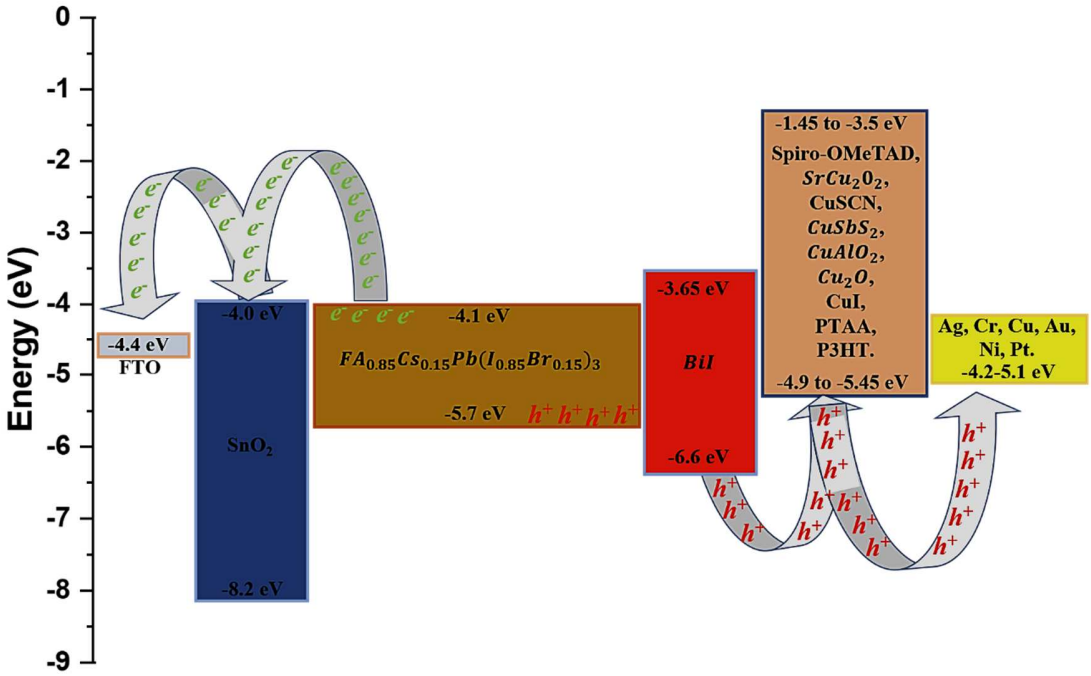

Fig. 2 Band alignments between ETL, different HTL's with perovskite absorber including BiI_3 IL.

Table I: Details of primary input parameters used for the simulation of $FAPI$ based perovskite solar cells.

Parameters	**FTO**	**ETL (SnO_2)**	**$FA_{0.85}Cs_{0.15}Pb(I_{0.85}Br_{0.15})_3$**	**BiI_3 (IL)**	**HTL (Spiro-OMETAD)**
Thickness (nm)	500	70 **(Karthick et al., 2020)**	500	30	150
Band gap (eV)	3.50	3.50	1.59	1.72 **(Coutinho et al., 2019)**	2.9
E Affinity	4.00	4.00	4.09 **(Prathapani et al., 2018)**	4.10 **(Lee et al., 2018)**	2.2
Permittivity	9.00	9.00	6.600	5.78 **(Brandt et al., 2015b)**	3.00
Effective density of states at CB	2.2×10^{18}	2.2×10^{17}	2.0×10^{19}	2.5×10^{19}	2.2×10^{19}
Effective density of states at VB	2.2×10^{18}	2.2×10^{17}	2.0×10^{18}	2.5×10^{19}	2.2×10^{19}
Mobility of e^-	20	20	8.16 **(Prathapani et al., 2018)**	600 **(Han et al., 2014)**	1.0×10^{-4}
Mobility of h^+	10	10	2	200 **(Callahan et al., 2018)**	1.0×10^{-4}
Density of n-type doping	1.0×10^{15}	1.0×10^{17}	1.3×10^{16}	1.0×10^{16}	0
Density of p-type doping	0	0	1.3×10^{16}	1.0×10^{16}	1.0×10^{18}
Density of defects	Donor-1.0×10^{18}	Donor – 1.0×10^{15}	Neutral-4×10^{13}	Neutral-1×10^{15}	Acceptor-1.0×10^{15}

3. Results and discussion

3.1 Ideal device performance

In this simulation, Firstly SnO_2 (ETL) and $Spiro-OMeTAD$ (HTL) based $FAPI$ perovskite ideal device performances are carefully investigated as a reference, which shows a PCE of 19.17 % with a short current density (J_{sc}) value of 22.24 mA/cm^{-2}, a fill factor (FF) of 67.46 %, and an open-circuit voltage (V_{oc}) of 1.27 V that is associated with previously reported results **(McMeekin et al., 2017; Yu et al., 2016).** Here, we used the SnO_2 as an ETL instead of TiO_2

and ZnO due to the excellent properties of SnO_2 **(Jiang et al., 2018; D. Liu et al., 2019)** and also, SnO_2 provides perfect band alignment with mixed cation/halide perovskite than TiO_2 **(Correa Baena et al., 2015).**

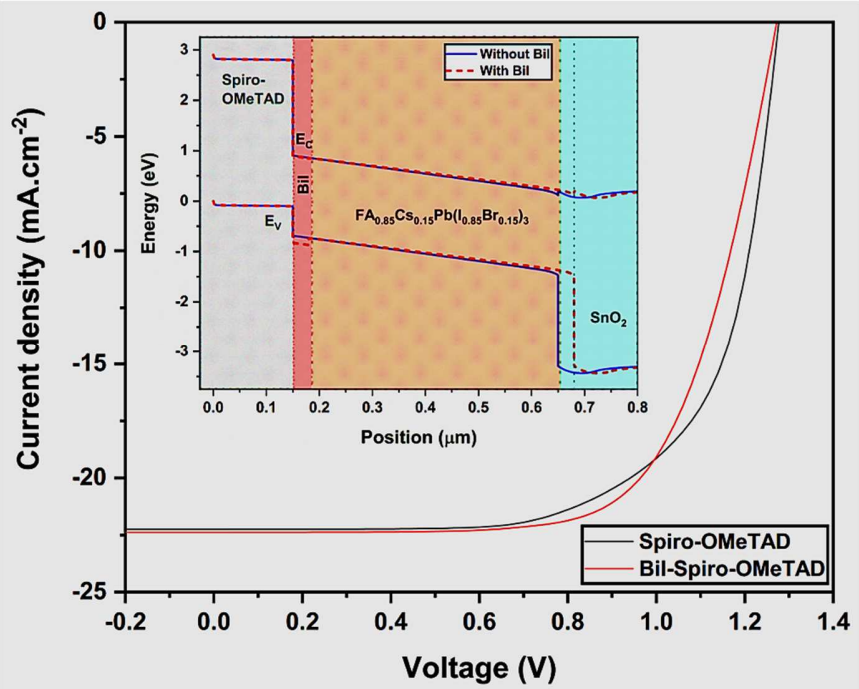

Fig. 3 Current density- voltage (J-V) characteristic curves of both ideal device structures (with and without BiI_3 IL). The inset represents the energy band diagram.

The primary and crucial job of the ETL layer is to extract the electron from the absorber layer and simultaneously blocking the holes to avoid recombinations. Experimentally, due to the different ETL layer thicknesses, the light transmittance of the film will vary. Therefore, the ETL layer thickness plays a vital role (Xiong et al., 2018). In general, SnO_2 – ETL layer needs a higher thickness than TiO_2 – ETL to completely cover the TCO substrate due to the larger size of SnO_2 nanoparticles (D. Liu et al., 2019). Fumin Li et al. studies demonstrate that the 66 nm SnO_2 – ETL device showing an improved PV performance than 34 nm and 48 nm ETL devices. The thicker ETL effectively blocks the hole transport, and it reduces the charge carrier recombination at the interfaces, which is beneficial for the device's performance (Li et al., 2018). Also, the 70 nm $Cl - SnO_2$ – ETL device provides an enhanced PCE than 40 nm and 90 nm layer contained devices due to tight interface contact with the TCO substrate and absorber (Duan et al., 2017).

Furthermore, it is well-known that several factors affect perovskite device performance, including HTL layer thickness. In this simulation, we used an optimized thickness of 150 nm for all different HTL layers. Previous experimental reports justify that the 180 nm HTL layer device offers a higher PV performance than other HTL thicknesses, such as 100, 250, 400, 450, 500, and 700 nm (Kim et al., 2015). Apart from the hole extraction and transportation, the absorber layer's safety and suppression of the interface defects are crucial to achieving good device performance. Therefore, the HTL thickness should be thicker than 150 nm to avoid direct contact between the

absorber and the electrode. Also, a thick HTL efficiently enhances the charge carrier collection due to an improved reflection from the smooth HTL/electrode interface; thus, the device efficiency is highly improved (Lei et al., 2018; Marinova et al., 2015).

Later, we introduced an additional thin BiI_3 IL in between the perovskite/HTL interface (see **Fig.1**). Perovskite/HTL interface engineering is a well-known strategy to efficiently passivate the defects, which generally promotes hole extraction by blocking the secondary electrons **(Gil-Escrig et al., 2015).** Surprisingly, here all the photovoltaic parameters are drastically enhanced, the obtained PCE improved from 19.17 % to 19.28 % ($J_{sc} = 22.38\ mA/cm^{-2}$, $FF = 67.73\ \%, and\ V_{oc} = 1.27$). **Fig. 3** illustrates the simulated current density – voltage curves (J-V) of both ideal device structures, and the inset's shows the energy band diagram. The obtained quantum efficiency (QE) graphs were displayed in the supplementary information (see **Fig. S1**). Experimentally, introducing IL is not only beneficial for stopping ion migration, and also it modifies the energy level alignment between the layers. In general, the interfacial energy level alignment influence the hole injection rate (i.e., perovskite/HTL interface). The energy barrier (EB) at the interfaces leads to charge carrier recombination losses restricting the charge transfer. The non-appearance of EB at the interfaces helps the smooth and fast charge transfer/injection and efficiently reduces the recombinations (Shao and Loi, 2020). In this case, BiI_3 has a higher bandgap value and larger conduction band than the absorber (see **Table I and Fig. 2**), leading to the favored energy level alignment that efficiently minimizes/reduces the EB at the HTL/perovskite interface.

Henceforth, introducing BiI_3 IL in the Perovskite/HTL interface facilitates the interfacial hole transport and possibly suppresses the interfacial charge recombination. The valence band offset (VBO) is generally defined as the difference between the e^- affinity and bandgap of the perovskite absorber; and e^- affinity and bandgap of the HTL (i.e., $VBO = e^-\text{affinity}_{HTL} - e^-\text{affinity}_{perovskite} + bandgap_{HTL} - bandgap_{Perovskite}$) **(Abdelaziz et al., 2020; Sahu and Dixit, 2018; Shasti and Mortezaali, 2019).** The negative VBO is obtained in the perovskite/$Spiro - OMeTAD$ interface (-0.58 eV), which signifies that the presence of recombination of minority charge carriers occurs in the interfaces **(Lin et al., 2019)**. After adding the BiI_3 IL, the VBO (i.e., $VBO = e^-\text{affinity}_{BiI_3} - e^-\text{affinity}_{HTL} + bandgap_{BiI_3} - bandgap_{HTL}$ **(Minemoto and Murata, 2015**)) turns positive (0.72 eV), by means that the band alignment is modified between the absorber and the HTL interface, which is beneficial for balanced charge carrier transfer; as a result, it boosts the FF value (see **Table S1**). Additionally, the current value of BiI_3 IL attached device is higher than that of the reference device, which generally leads to higher charge carrier mobility, helping further PCE improvement.

Hence, it is clear that the BiI_3 IL influences the device results, so in the following sections, we are going to check the device performances based on several HTL candidates with and without BiI_3 IL to understand the interfacial layer effect. Finally, we will correlate the influence of the BiI_3 IL thickness with the perovskite absorber layer thickness and also the effect of parasitic resistances, using the most appropriate HTL system.

3.2 Effect of different HTL's with and without BiI_3 IL

Experimentally, $Spiro-OMeTAD$ HTL needs some external doping (such as tri-tert-butyl-pyridine (tBp), lithium bis-tri-fluoro-methane-sulfonimide (Li-TFSI), and other cobalt salts) to improve the internal charge mobility, but at the same time, it is rising the interface recombination, which led to poor device performance **(Gheno et al., 2016**). Therefore, finding alternative low-cost and stable HTL is essential to improve device efficiency. Hence, in this section, several HTL ($Cu_2O, CuI, CuAlO_2, CuSbS_2, SrCu_2O_2, CuSCN, PTAA, P3HT$) candidates are studied and presented. Input parameters of the mentioned HTL materials are listed in Table II. By using 70 nm of SnO_2 as an ETL and switching different HTL materials with and without BiI_3 IL, the comparative energy band diagram is illustrated in **Fig. 4** and **Fig. S2**. Obtained J-V characteristic curves, as well as the appropriate energy band diagrams (inset) for all mentioned HTL devices, are presented in **Fig. 5, Fig. 6**, and **Fig. S3 - Fig. S8**, respectively.

Table II: Input parameters for proposed different HTL materials.

Parameters	**$SrCu_2O_2$**	**Cu_2O**	**$CuAlO_2$**	**CuSCN**	**$CuSbS_2$**	**CuI**	**PTAA**	**P3HT**
Thickness (nm)	150	150	150	150	150	150	150	150
Bandgap (eV)	3.3	2.17	3.46	3.2	1.58	2.98	2.96	1.8
E Affinity	2.2	3.2	2.5	1.9	4.2	2.1	2.3	3.9
Permittivity	9.77	7.1	60	10	14.6	6.5	9	3
Effective density of states at CB	2.0×10^{20}	2.1×10^{17}	2.0×10^{20}	2.2×10^{19}	2.2×10^{18}	2.8×10^{19}	2.0×10^{21}	2.0×10^{20}
Effective density of states at VB	2.0×10^{21}	1.0×10^{19}	1.0×10^{22}	1.8×10^{19}	2.2×10^{19}	2.0×10^{19}	2.0×10^{21}	2.0×10^{20}
Mobility of e^-	0.1	200	2	1.0×10^{-4}	49	100	1	1.0×10^{-4}
Mobility of h^+	0.46	80	8.6	1.0×10^{-1}	49	43.9	40	1.0×10^{-3}
Density of n-type doping	0	0	0	0	0	0	0	0
Density of p-type doping	1.0×10^{17}	1.0×10^{18}	1.0×10^{20}	1.0×10^{18}	1.0×10^{18}	1.0×10^{18}	1.0×10^{18}	1.0×10^{18}
Density of defects	Acceptor-1.0×10^{15}	Acceptor-1.0×10^{15}	Acceptor-1.0×10^{15}	Acceptor-1.0×10^{15}	Acceptor-1.0×10^{15}	Acceptor-1.0×10^{15}	Acceptor-1.0×10^{15}	Acceptor-1.0×10^{15}
References	**(Shasti and Mortezaali, 2019)**	**(Shasti and Mortezaali, 2019) (Lin et al., 2020)**	**(Shasti and Mortezaali, 2019)**	**(Azri et al., 2019) (Chakraborty et al., 2019)**	**(Devi and Mehra, 2019)**	**(Coulibaly et al., 2019) (Azri et al., 2019)**	**(Coulibaly et al., 2019)**	**(Coulibaly et al., 2019) (Azri et al., 2019)**

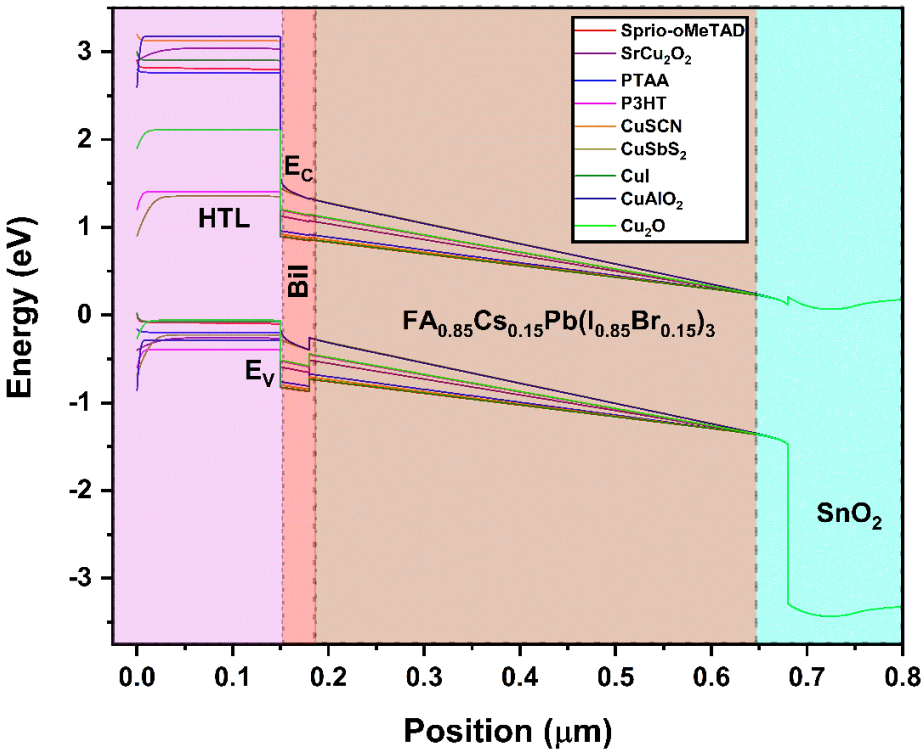

Fig. 4 Energy band diagram for the reference device including BiI_3 IL with different HTL candidates.

After testing several HTL candidates over the same configured structure, we noticed that the Cu_2O-HTL based device shows a remarkable PCE of 23.07 % than other competitors due to their excellent hole mobility value (Table II) and the energy band alignment with the absorber layer (**see Fig. 5**). The obtained FF value (81%) is highly improved compared to the reference $Spiro-OMeTAD$-HTL device (67 %), which can be attributed to the promotion of hole conduction through the HTL. The simulated photovoltaic parameters of all different HTL based device results are illustrated in Table III. The VBO is significantly improved (- 0.31) while using Cu_2O-HTL instead of $Spiro-OMeTAD$, that could be a good reason for the enhanced device performance. After adding the BiI_3 IL in between the Perovskite/Cu_2O-HTL interface, as we expected, the overall device performance increased from 23.07 % to 23.29 % compared to the standard device (**see Fig. 5** and Table III) due to the positive VBO (0.45 eV). The VBO value of BiI_3/Cu_2O interface is lower than the $BiI_3/Spiro-OMeTAD$ interface, yet the device performance is boosted because of the high VBO, which acts as a barrier for the hole diffusion **(Minemoto and Murata, 2015)** and lead to lower performance (i.e., $Spiro-OMeTAD$-HTL device). Also, hole mobility plays a massive role in efficiently extracting and surpassing the holes from the absorber to HTL and the electrode (Table II). For example, in a real device, Elesman *et al.* experimental TRPL results explain the Cu_2O/perovskite films exhibit excellent lifetime than P3HT/perovskite films, which signifies that the Cu_2O/perovskite interface gains more hole extraction than P3HT/perovskite interface **(Elseman et al., 2019)**. The $SrCu_2O_2$ – HTL device having the second-highest efficiency of 22.75 %, here also the VBO is negative (-

0.18 eV) but it is better than the $Spiro-OMeTAD$ and Cu_2O-HTL's, at the same time, the hole mobility is lower than the Cu_2O and higher than $Spiro-OMeTAD$ (Table II). The addition of BiI_3 IL furthermore improves the VBO to 0.32 eV, which enhances the device performance from 22.75 % to 23.20 % (**see Fig. 6**), it is higher than the previously simulated perovskite device results (Table III). The $PTAA$-HTL based device showed PCE of 19.80 %, which is attributed to the VBO (- 0.42 eV) and hole mobility value, it is finer than $Spiro-OMeTAD$-HTL. While adding the BiI_3 IL, the VBO is considerably enhanced (0.56 eV), which directed towards the higher performance from 19.80 % to 20.15 % due to an enhancement in the interface (**see Fig. S3**). The previously reported simulated PTAA-HTL device shows higher efficiency (23.5 %) than the current device results because of the higher HTL thickness (1000 nm) and the J_{sc} value (41.03 mA/cm^{-2}) **(Coulibaly et al., 2019).** $CuAlO_2$-HTL based device displays 19.98 % of efficiency due to the reduced charge transfer resistance between HTL and the electrode **(Igbari et al., 2015)**, the obtained performance is higher than the reference $Spiro-OMeTAD$-HTL device (Table III). In this case, the VBO is positive (0.28 eV) compared to formerly discussed HTL contenders; surprisingly, after including BiI_3 IL, the VBO turns into negative (- 0.14 eV), as a consequence, the V_{oc} value is significantly reduced. Even though, the performance is slightly increased from 19.98 % to 20.04 % due to an enrichment in short-circuit current (**see Fig. S4,** and Table III). $CuSbS_2$-HTL device demonstrating the PCE of 19.08 %, here also the VBO is positive (0.1 eV), while adding BiI_3 IL, the VBO value is reduced a little bit (0.04 eV), which is reflecting in the FF result; however, the PCE is slightly improved (**see Fig. S5,** and Table III). Previous SCAPS reports shows that a higher efficiency was obtained using $CuSbS_2$-HTL (24.1 %) because of the larger J_{sc} value (31.7 mA/cm^{-2}) and the HTL thickness (438 nm), **(Devi and Mehra, 2019)** is much larger than the current result (22.6 mA/cm^{-2}), shown in Table III. $CuSCN$-HTL device displaying PCE of 19.05 %, the VBO is negative (-0.58 eV), after adding BiI_3 IL, the VBO is significantly improved to 0.72 eV, at the end, the FF is reduced due to the higher VBO, but the device shows the same performance because of the improvement in the J_{sc} value (**see Fig. S6,** and Table III). Previous report shows that the device performance is not entirely associated with perovskite/$CuSCN$ interface rather than $CuSCN$/electrode **(Arora et al., 2017).** Therefore, we will demonstrate the effect of HTL with different electrodes in the following sections. But in reality, experimental $CuSCN$-HTL contained device demonstrates excellent thermal degradation stability than well known $Spiro-OMeTAD$-HTL due to the strong resistance against environmental stress **(Jung et al., 2016).** CuI-HTL device exhibiting PCE of 18.81 %, the VBO is negative (-0.6 eV), after inserting BiI_3 IL, the VBO is drastically increased (0.74 eV), the performance is also improved minorly but not more (i.e., 18.81 % to 18.86 %) (**see Fig. S7** and Table III), the high VBO might restrict the further improvement as we discussed before. Noticeably, $P3HT$-HTL device showing the lowest photovoltaic performance (17.99 %) among all HTL's due to the lower hole mobility value and the lower VBO (0.02 eV). According to the previous report, the significant mismatch between the quasi-Fermi level splitting (QFLS) to V_{oc} affects the results that occur while using the $P3HT$-HTL compared to $PTAA$-HTL, enhancing the interfacial recombination at the interfaces (Caprioglio et al., 2019) might be another reason for the lower performance. After including the BiI_3 IL, the VBO is changed (0.12 eV), but surprisingly, the FF and V_{oc} values are droped, it further reduces the performance (**see Fig. S8,** Table III). Overall, other HTL based device exhibits lower performance than these two

(Cu_2O & $SrCu_2O_2$) with and without BiI_3 IL. According to the previous report, the vacancy formation energies are reduced in the order of $Cu_2O < SrCu_2O_2 < CuAlO_2$ and it affects the conduction properties; mainly, it modifies the acceptor defects. The vacancy distribution in Cu_2O impacts the bandgap, and the conduction properties **(Nolan, 2008)**. Our simulated device results are compared with recently published reports, shown in Table III. It emphasizes that the simulated device performance is solely based on the appropriate absorber layer, ETL, HTL arrangement, and energy band alignment **(Azri et al., 2019; Coulibaly et al., 2019; Elseman et al., 2019; Lin et al., 2020; Shasti and Mortezaali, 2019; Zheng et al., 2017).** Therefore, the simulated device with BiI_3 IL efficiently boosting up most of the above-mentioned HTL's based device performances compared to the referenced device, especially, the J_{sc} and FF values are improved (Table III). The obtained QE behavior of $Spiro-OMeTAD$-HTL referenced device is nearly similar to the BiI_3 IL contained device, shown in **Fig. S1**. Hence, it is an evident that the BiI_3 IL with suitable HTL (Cu_2O & $SrCu_2O_2$) directly influences the device performance. In the following sections, we will examine the various electrodes with and without BiI_3 IL (using different HTL's) to understand the effect over the HTL/electrode interface.

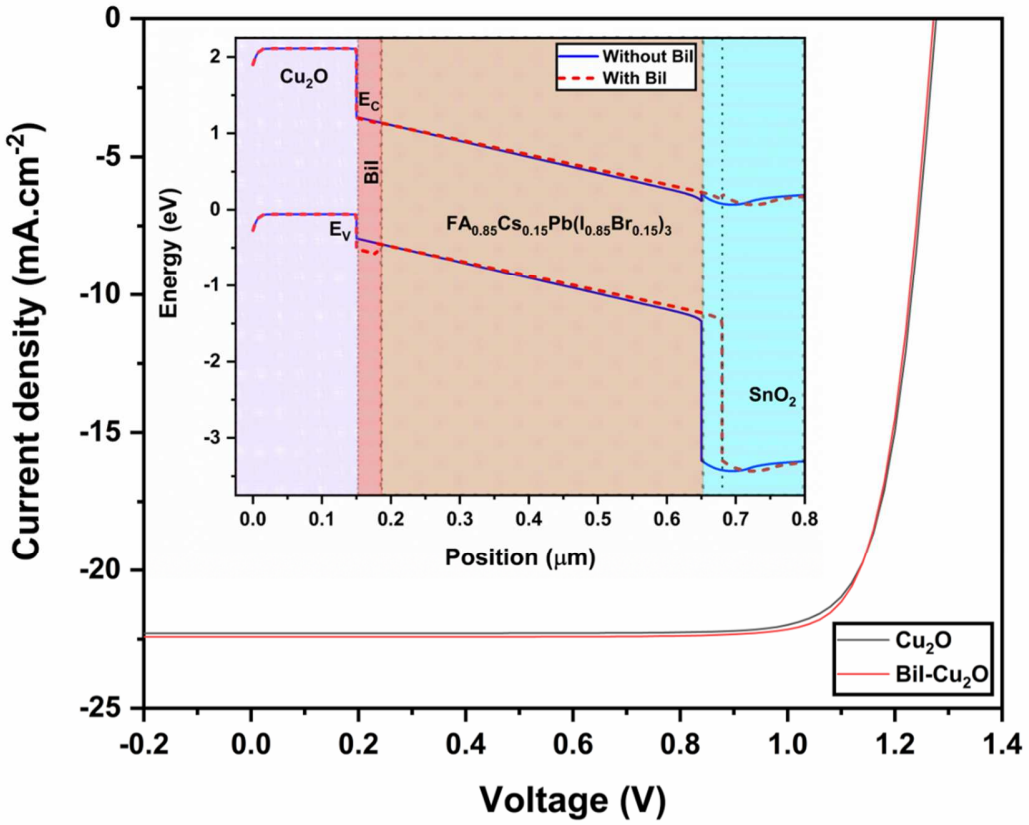

Fig. 5 shows the Current density- voltage (J-V) characteristic curves of both ideal device structures (with and without BiI_3 IL) with Cu_2O-HTL. The insets represent the energy band diagram.

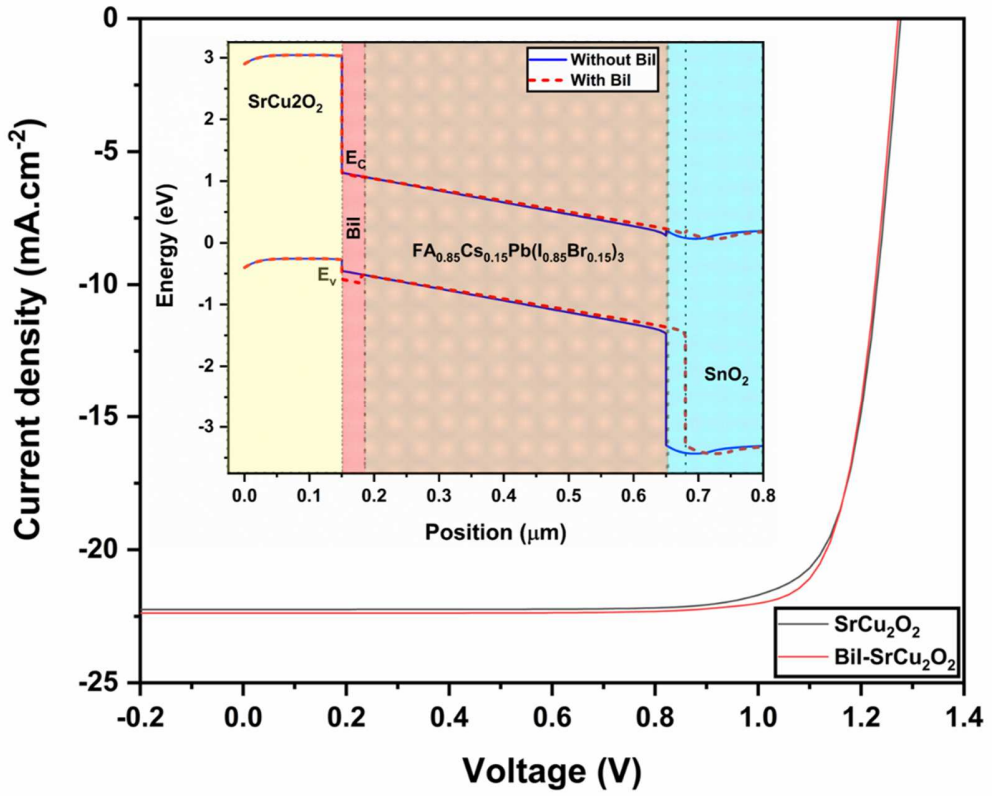

Fig. 6 shows the Current density- voltage (J-V) characteristic curves of both ideal device structures (with and without BiI_3 IL) with $SrCu_2O_2$ – HTL. The insets represent the energy band diagram.

Table III: Recorded photovoltaic parameters for proposed different HTL materials.

HTL		J_{sc} (mA/cm^{-2})	FF (%)	V_{oc} (V)	PCE (%)
$SrCu_2O_2$	W/o BiI_3	22.25	80.09	1.27	22.75
	W BiI_3	22.38	81.46	1.27	23.20
(Shasti and Mortezaali, 2019)		23.22	78.50	1.11	20.29
Cu_2O	W/o BiI_3	22.29	81.04	1.27	23.07
	W BiI_3	22.42	81.65	1.27	23.29
(Shasti and Mortezaali, 2019)		23.26	78.50	1.10	20.14
(Elseman et al., 2019)		22.53	67.36	1.13	17.23
(Lin et al., 2020)		18.41	81.73	1.06	16.03
$CuAlO_2$	W/o BiI_3	22.24	70.46	1.27	19.98
	W BiI_3	22.38	70.62	1.26	20.04
(Shasti and		23.23	78.40	1.12	20.32

Mortezaali, 2019)					
CuSCN	W/o BiI_3	22.25	67.05	1.27	19.05
	W BiI_3	22.38	66.92	1.27	19.05
(Lin et al., 2020)		18.28	76.34	1.08	15.18
(Azri et al., 2019)		21.89	83.70	1.27	23.30
$\boldsymbol{CuSbS_2}$	W/o BiI_3	22.60	84.74	0.99	19.08
	W BiI_3	22.77	84.68	0.99	19.15
(Devi and Mehra, 2019)		31.70	81.0	0.94	24.10
CuI	W/o BiI_3	22.25	66.22	1.27	18.81
	W BiI_3	22.38	66.25	1.27	18.86
(Lin et al., 2020)		18.29	79.44	1.08	15.79
(Azri et al., 2019)		21.89	83.21	1.27	23.14
PTAA	W/o BiI_3	22.24	69.68	1.27	19.80
	W BiI_3	22.38	70.75	1.27	20.15
(Coulibaly et al., 2019)		41.03	74.14	0.77	23.58
P3HT	W/o BiI_3	22.26	67.10	1.20	17.99
	W BiI_3	22.40	66.31	1.19	17.72
(Coulibaly et al., 2019)		32.25	75.05	0.74	17.98
(Azri et al., 2019)		21.89	74.05	1.27	20.61

3.3 Effect of different electrodes with and without $\boldsymbol{BiI_3}$ IL

In this section, the impact of various electrodes such as silver ($Ag - 4.26\ eV$), chromium ($Cr - 4.5\ eV$), copper ($Cu - 4.65\ eV$), gold ($Au - 5.10\ eV$), nickel ($Ni - 5.15\ eV$), platinum ($Pt - 5.65\ eV$) contained device performances were carefully investigated. The electrode work function (WF) values are taken from the previous reports **(Behrouznejad et al., 2016; Ming et al., 2018).** The energy band diagrams of typical and BiI_3 IL included different HTL solar cells with various WF electrodes are depicted in **Fig. 7** and **Fig. S9**. The band diagram shows that the Au, Ni, and Pt lines are overlapped due to their work function value lies between 5.1 eV to 5.65 eV which is associated with their higher build in voltage behavior (V_{bi}) **(Lin et al., 2020; Minemoto and Murata, 2014).** Other candidates such as Ag, Cr, and Cu, demonstrates the different alignment due to their lower V_{bi} and their work function values (4.2 eV to 4.65 eV) **(Lin et al., 2020).**

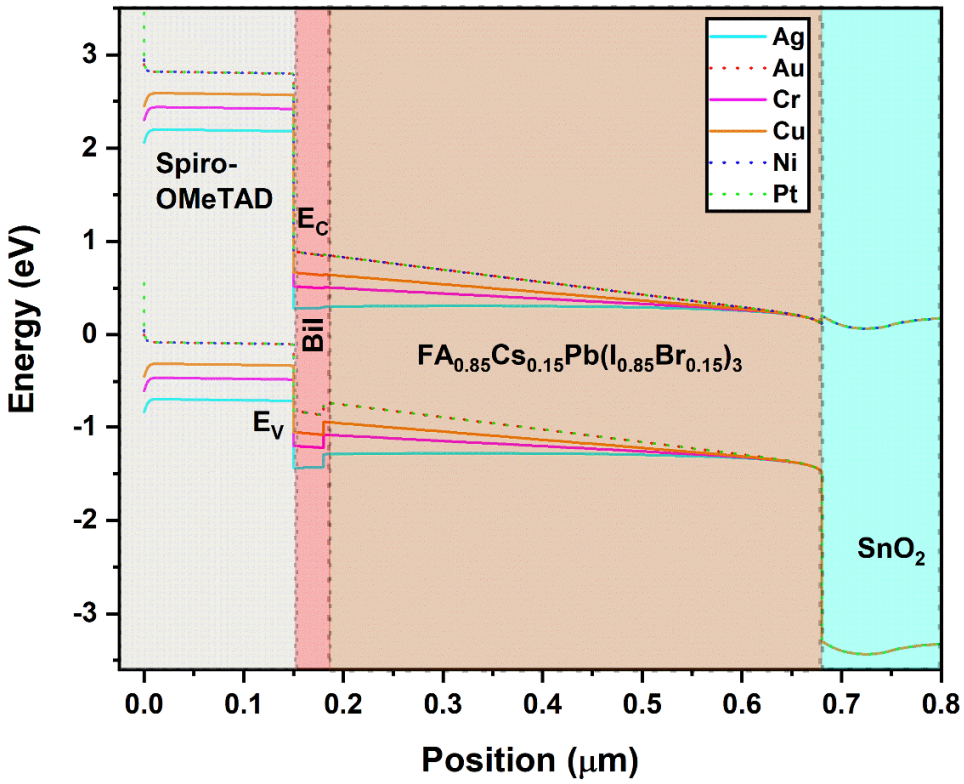

Fig. 7 Energy band diagram for the reference device including BiI_3 IL with different electrodes.

Fig. 8 demonstrates that the obtained photovoltaic parameters $(J_{sc}, V_{oc}, FF, and\ PCE)$ of the typical devices with different HTL's, especially using various electrodes based on their WF values**.** Apart from the Perovskite/HTL interface, the energy level mismatch alignment between the HTL/electrode interface also decides the device performance **(Z. Wu et al., 2019; Zheng et al., 2017).** The $CuSbS_2$-HTL device possesses the highest J_{sc}, and FF values, at the sametime, it has the poor V_{oc} results than other HTL candidates. The enhanced electric field throughout the perovskite layer occurred while increasing the electrode WF value. In general, the reduced device performance corresponding to the high Schottky barriers at the HTL/electrode interface, which restricts the hole extraction **(Lin et al., 2020, 2019).** Most of the HTL's based devices showing similar PCE values for $Ni, and\ Pt$ electrodes, except for $CuAlO_2, CuSbS_2, PTAA,$ and $P3HT$ (**Fig. 8 (d)** and Table S.II). The above mentioned HTL devices exhibits entirely enhanced photovoltaic parameters demonstrated in **Fig. 8**. It is evident that either higher or lower electrode WF directly influences the results, and also, it is related to HTL properties (i.e, hole mobility and VBO). The obtained quantum efficiency curves for typical devices are illustrated in **Fig. S10 (a)**. Simulated Ag-electrode device presenting the lower QE compared to other electrode devices, and it increases significantly based on the electrode WF values. From the QE graphs, it is easier to understand that the $Au, Ni,$ and Pt electrodes displaying the same behavior, the lines are overlapped which agrees the band diagram result (**see Fig. 7**). Previous reports exhibits that the oxidation from silver (Ag) to silver iodide (AgI) or silver bromide $(AgBr)$ due to the ion imgiration from perovskite layer through the HTL influence the device result. Also, the low

formation energy (FE) and the low diffusion barrier (DB) value (0.27 eV) of Ag compared to other electrodes which manipulates the device performance **(Behrouznejad et al., 2016; Kato et al., 2015; Ming et al., 2018; Svanström et al., 2020).** The Cu has much better corrsion resistance and improved DB value (0.42 eV) than Ag, even though it is not diifused into the perovskite layer. Therefore, Cu device performance was much better than Ag devices **(Ming et al., 2018; Zhao et al., 2016).** The higher DB value (0.83 eV), and the lower FE of Cr helps to enhance the PCE than Ag, meanwhile, the R_{Series} might be rising because of their high resistivity value **(Ming et al., 2018).** Due to the improved WF value from Ag, Cr to Cu electrodes (**see Fig. 7**), it is clear that the holes efficiently transferred from HTL to electrode, and it influence the device performances (**see Fig. 8**) Possibly, the higher recombination problem occurs at the perovskite/HTL or HTL/electrode interfaces in $Ag, Cr,$ and Cu based devices than Au, Ni, and Pt devices. The higher WF electrode devices exhibit excellent photovoltaic parameters than others (see **Fig. 8**) **(Behrouznejad et al., 2016).** Therefore, it is recommended that the higher WF electrodes such as Au, Ni, and Pt, are more suitable candidates for mixed cation/halide perovskite solar cells.

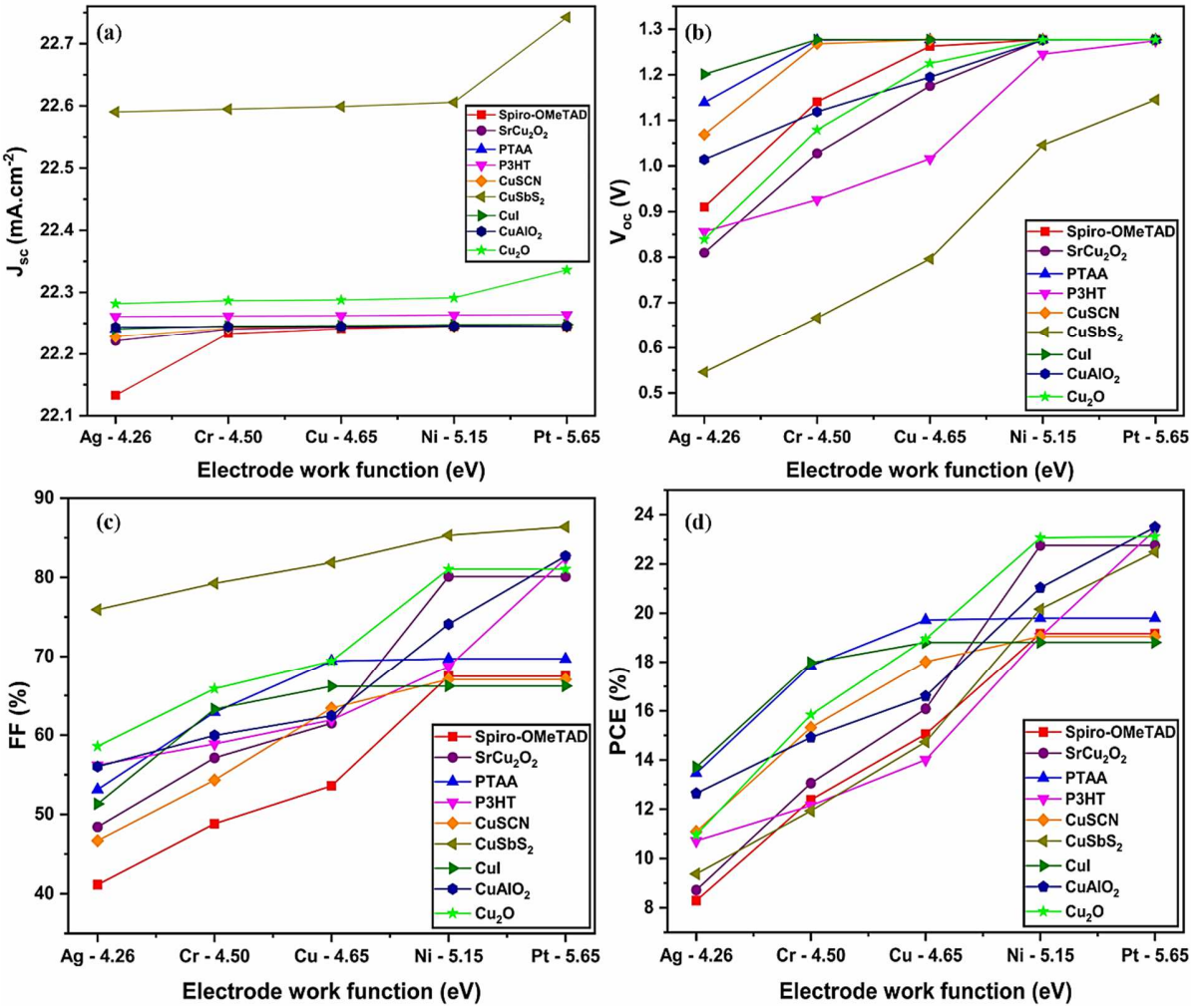

Fig. 8 The photovoltaic parameters (J_{sc}, V_{oc}, FF, PCE) for the reference device with different HTL's and electrodes.

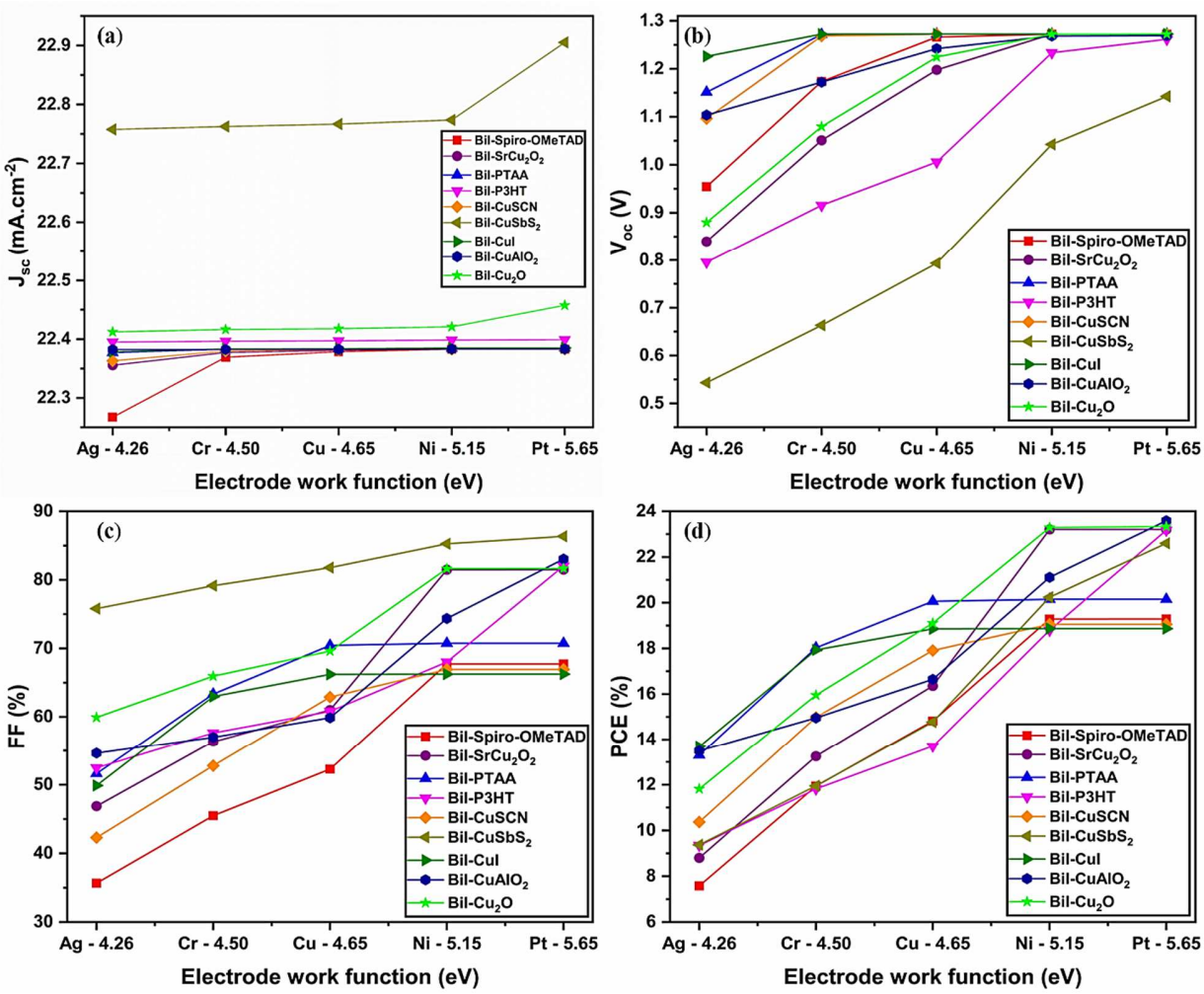

Fig. 9 The photovoltaic parameters (J_{sc}, V_{oc}, FF, PCE) for the BiI_3 IL contained devices with different HTL and electrodes.

The obtained photovoltaic parameters ($J_{sc}, V_{oc}, FF, and\ PCE$) for the BiI_3 IL devices with different HTL and electrodes, shown in **Fig. 9**. The obtained QE curves for the reference device, including IL, is demonstrated in **Fig. S10**. After adding the BiI_3 IL, we noticed that the device performance significantly improved while using higher WF electrodes (Au, Ni, and Pt). Simultaneously, the $Spiro-OMeTAD$-HTL devices show a decrement in photovoltaic parameters for Ag, Cr to Cu electrodes due to their lower WF value as well as it possibly creates the high Schottky barrier at the HTL/electrode interface which reduce the hole transport from HTL to an electrode. (Table S.II) The case of $P3HT$-HTL devices (for all anodes) demonstrates a slightly lowered performance than the normal one. Most HTL candidates prove that a thin BiI_3 IL efficiently enhances the device results with all the electrodes mentioned above. The device

performance is strongly affected due to the formation of the resistance layer at the HTL/electrode interface, so it is crucial to use the appropriate valence and conduction band energy levels having HTL **(Behrouznejad et al., 2016).** Moreover, the reported experimental result shows that placing a thin Cr interfacial layer inbetween HTL and Au interface significantly reduced the electrode diffusion at the higher temperature, which is beneficial for higher performance devices **(Domanski et al., 2016).** Therefore, adding an IL between the interfaces could be an excellent strategy to improve solar cell performance. In the following section, we will demonstrate the influence of BiI_3 IL thickness over the absorber layer thickness.

3.4 Effect of BiI_3 IL and absorber layer thickness

Generally, the properties of the perovskite absorber layer determine the device's performance. Mainly, the layer thickness is one of the leading parameter to enhance photon absorption, significantly improving the device results. After careful investigation, the Cu_2O-HTL was selected to perform the mentioned thickness analysis. Therefore, in this section, the influence of the perovskite layer and the BiI_3 IL thickness over the Cu_2O-HTL based device performance was carefully investigated. The absorber layer thickness differs from 500 to 1000 nm, as well as the interfacial layer thickness varied from 10 to 100 nm, and the other listed parameters in Table I remain the same.

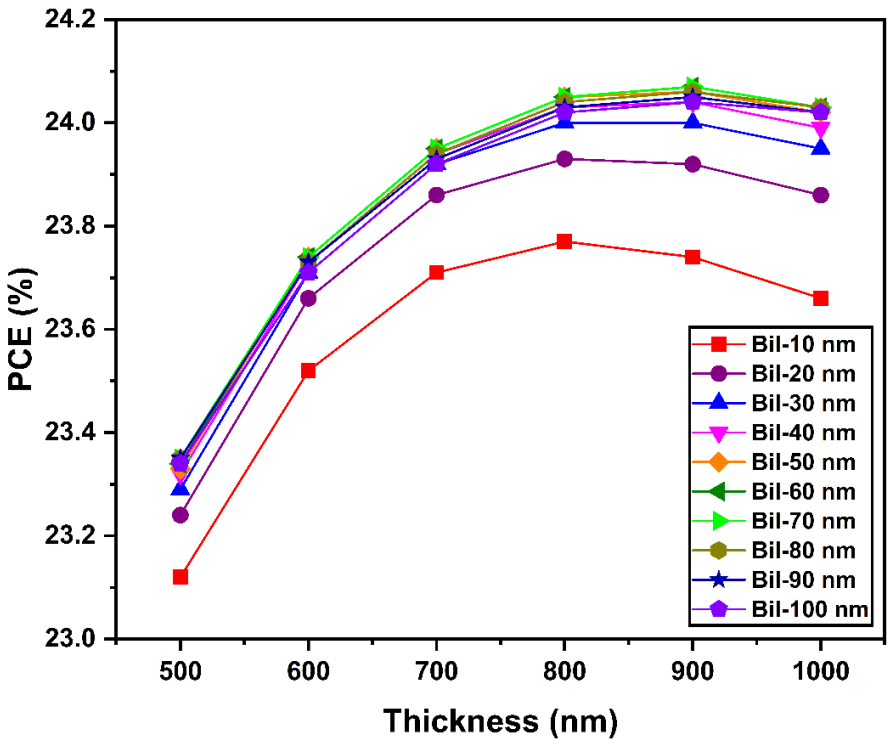

Fig. 10 The variation of PCE (a) with different perovskite layer (500 nm to 1000 nm) and BiI_3 IL (10 nm to 100 nm) thickness.

Fig. 10 demonstrates that the device PCE considerably enhances (23 % to 24 %) while increasing the absorber layer thickness from 500 to 1000 nm. It continuously improves up to 900 nm, then

slightly decreases. Several experimental reports reveal that a thick perovskite layer will absorb more photons, especially in the red to the near-infrared region (Chen et al., 2017; Yuan et al., 2016), which is appropriate for solar devices. For example, Jiehuan Chen et al. studied the solar cell performance based on the different perovskite layer thickness, especially beyond 700 nm (i.e., 700, 850, 1000, 1150, 1400, and 1650 nm) using a simple hot casting method (Chen et al., 2018). The 850 nm thicker absorber perovskite device provides the highest PCE (19.54%) among all other absorbers. Noticeably, the device maintains the stable PCE value of 19% from 700 to 1150 nm thickness range, and the device holds 80% of its initial PCE after 30 days. Therefore, using an optimum thicker perovskite absorber and the IL is beneficial for device improvement (Sanehira et al., 2016; S. Wu et al., 2019). Shaohang Wu et al. studied the inverted perovskite solar cell PV performance and stability while inserting a bismuth (Bi) interlayer (thickness - 5, 10, 20,40, and 80 nm) (S. Wu et al., 2019). The results show that the thicker Bi film offers a uniform and good coverage film than a thin layer. Due to increased contact resistance, a thicker Bi layered (i.e., 40 nm) solar cell reduces the device efficiency; most importantly, thicker IL lessens the degradation induced from ambient moisture leading to the stability enhancement (6000 h).

In that perspective, we simultaneously investigated the BiI_3 IL thickness with different perovskite layer thickness and makes it evident that the increment substantially improves the PCE (see **Fig. 10**). So, the optimum BiI_3 IL thickness was found at 70 nm, which corresponds to the superior PCE (i.e., PCE = 24.07%, J_{sc} = 24.18 mA/cm^{-2}, FF = 80.25%, and V_{oc} = 1.24 V). Moreover, the thick perovskite (more than 900 nm) layered device possibly suffered from higher recombination issues at the interface due to the absorber thickness that is larger than the diffusion length of charge carriers, which led to poor device performance. **Fig. 11** exhibits that the obtained QE graph's tendency is consistent with the PCE results (see **Fig. 10**). The current density – voltage characteristics (inset) also proves the previously mentioned behavior.

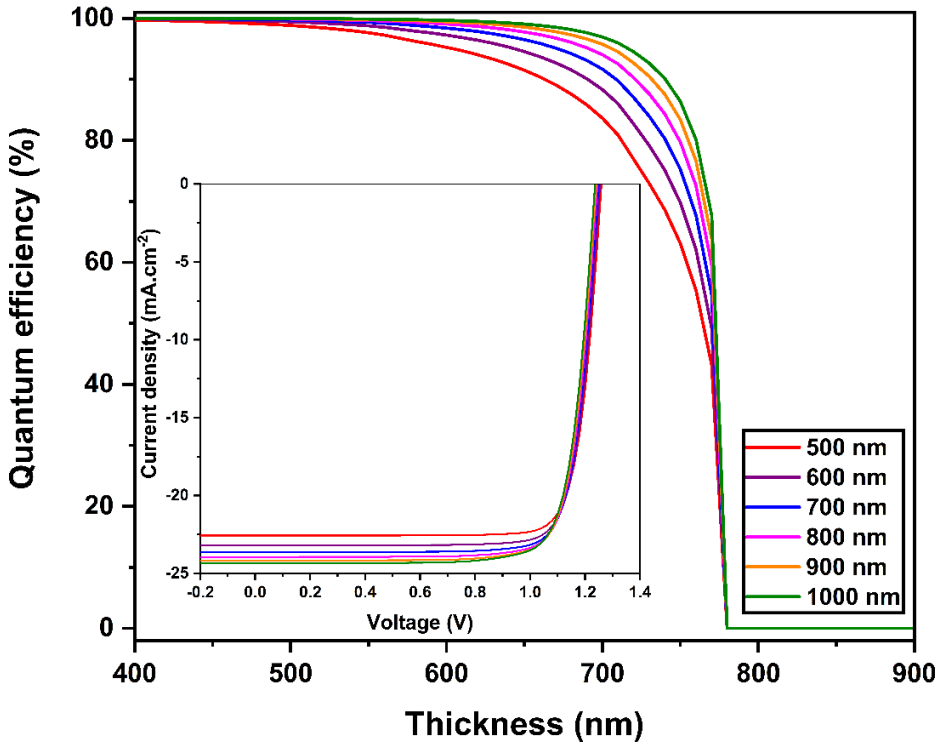

Fig. 11 QE and J-V characteristics (inset) of a different perovskite absorber layer thickness (500 nm to 1000 nm), including 70 nm of BiI_3 IL.

The simulation findings suggest that the 900 nm perovskite layer with 70 nm BiI_3 IL is appropriate for an excellent $FAPI$ based perovskite device. However, the parasitic resistances (R_{series} and R_{shunt}) are largely influence the experimental device performance. For example, a higher efficiency device must be having a low R_{series} and a high R_{shunt}. Our previous work clearly demonstrates that the effect of these resistances over three different perovskite absorber layer based devices (**Karthick et al., 2020**). Therefore, here we investigated the impact of these resistances over the Cu_2O-HTL device to understand the device behavior. We varied the R_{series} and R_{shunt} values between 10 – 80 $\Omega.cm^2$ and 1000 – 5000 $\Omega.cm^2$, respectively, and the corresponding evolution of the photovoltaic parameters are demonstrated in Fig. 12 (a) and (b). Our obtained results show that an increase in R_{series} from 10 to 80 $\Omega.cm^2$ strongly decreases the FF from 63% to 25%. Moreover, for a R_{series} over 40 $\Omega.cm^2$, J_{sc} is rapidly reduced from 24 to 14 mA/cm^{-2}And the overall PCE is rapidly decreased from 24% to only 4.5% (see **Fig.12 (a)**). Usually, R_{series} does not influence the V_{oc}, and the obatined V_{oc} behavior is shown in **Fig.12 (a)**. In comparison, increasing R_{shunt} enhances the FF and PCE values (see **Fig.12 (b)**), at the same time, it's slightly affects the V_{oc} and J_{sc} values. So, the high R_{shunt} is a indication of less defect and interface states presence in the device. While varying the R_{series} and R_{shunt} values into the optimized device considerable changes occur in the photovoltaic parameters. Therefore, it is clear that these parasitic resistances efficiently affect device performance.

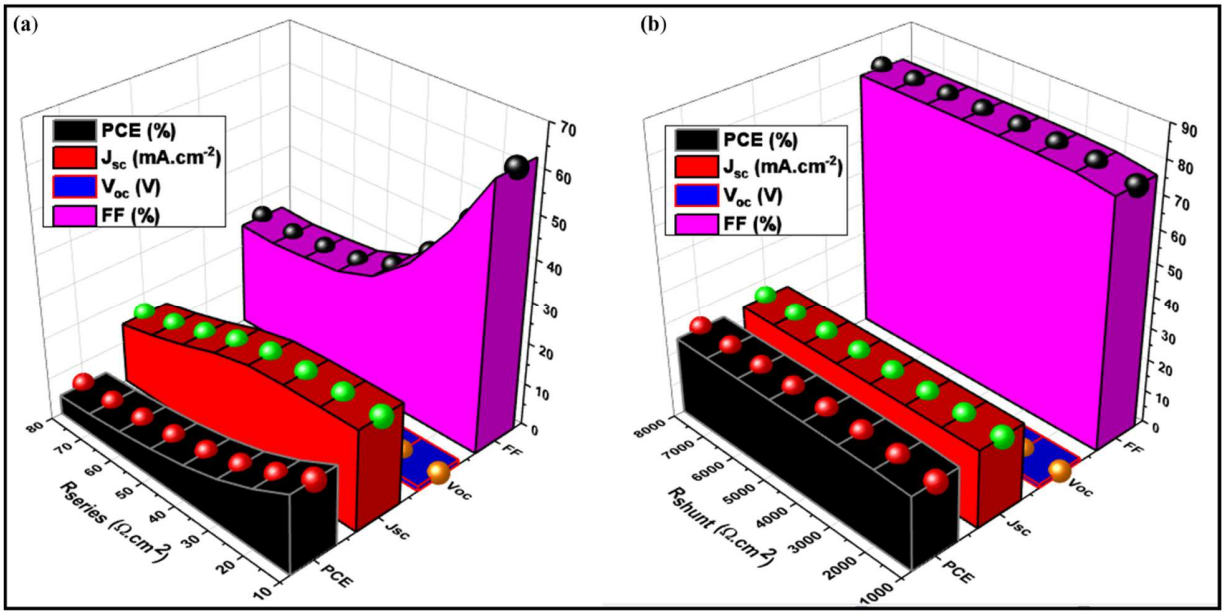

Fig. 12 Effect of R_{series} (a) and R_{shunt} (b) in the performance of simulated Cu_2O-HTL device including BiI_3 IL.

Finally, we also employed the optimized thicknesses (absorber and IL layer) in $SrCu_2O_2$-HTL solar cell and it shows a PCE of 23.91 % with a short current density (J_{sc}) value of 24.17 mA/cm^{-2}, a fill factor (FF) of 79.73 %, and an open-circuit voltage (V_{oc}) of 1.24 V.

In the end, this paper does not address any recombination issues (such as first, second, and third-order), which generally occurs in the real perovskite device. From the experimental point of view, the following points are crucial for boosting the actual perovskite device performance, such as (1) enhancing the absorber layer phase and its morphology, (2) improving the charge transport behavior, (3) passivating the surface nor interface defects, (4) altering the energy level alignment between the ETL/perovskite and perovskite/HTL interfaces, (5) improving the stability, (6) reducing the hysteresis. In general, to remove the traps at the interfaces is beneficial for the charge transfer. In that case, an interlayer's addition to the device helps to minimize the traps and suppress the ion immigration. Therefore, interface modifications and the chosen interfacial material directly influences the device stability, performance, and hysteresis behavior. Adding polymers, small molecules, 2D materials, or self-assembled monolayers (SAM) in between the perovskite/HTL interface efficiently may improve the charge transfer from the absorber to HTL and electrode **(Shao and Loi, 2020).** As a result, based on our report, a further insightful experimental study is necessary to understand the mechanism behind the BiI_3 IL over the device performance.

4. Conclusion

In this work, for the first time $FA_{0.85}Cs_{0.15}Pb(I_{0.85}Br_{0.15})_3$ perovskite absorber layer based n-i-p planar device with and without BiI_3 interfacial layer tested with different HTL's and various electrodes, which was carefully analyzed and presented using SCAPS. The simulated results exhibit that the Cu based HTL's, especially Cu_2O & $SrCu_2O_2$ shows excellent photovoltaic

performance than other HTL competitors. The optimized 900 nm perovskite layer with a thin (70 nm) interfacial BiI_3 layer has a more substantial influence on the solar cell results, which significantly boosted the photovoltaic parameters by reducing the perovskite/HTL interface defects. Therefore, both Cu_2O and $SrCu_2O_2$ HTL's are considered as suitable HTL's (with and without BiI_3 IL) for $FA_{0.85}Cs_{0.15}Pb(I_{0.85}Br_{0.15})_3$ based planar device. Also, the impact of different electrodes was examined using various HTL candidates, and our results emphasize that the higher work function electrodes such as Au, Ni, and Pt are more considerable than Ag, Cr to Cu. From the result, the simulated device displaying an efficiency of around 24 % with a suitable Cu_2O-HTL. Here, the absence of parasitic electrical losses (without considering the optical reflectance of each layer at the interface nor surface) could be the prominent reason for the obtained higher efficiency than the reported experimental reports. The optimized absorber, IL thickness, and parasitic resistances are also crucial for efficient devices. These simulation findings are useful for further understanding of the BiI_3 IL in between perovskite/HTL interface and enhancing the mixed cation/halide perovskite solar cells.

Acknowledgments

S. Karthick, thankful to CONACYT for the doctoral fellowship grant. This work is partially supported by the project CONACyT-SENER 263043 and also profited from the French government support managed by the National Research Agency under the Investments for the Future program with the reference ANR-10-LABX-0074-01 Sigma-LIM. S. K and J.B. are thankful to the PLATINOM technology platform (common facility of the University of Limoges).

References

Abdelaziz, S., Zekry, A., Shaker, A., Abouelatta, M., 2020. Investigating the performance of formamidinium tin-based perovskite solar cell by SCAPS device simulation. Opt. Mater. (Amst). https://doi.org/10.1016/j.optmat.2020.109738

Arora, N., Dar, M.I., Hinderhofer, A., Pellet, N., Schreiber, F., Zakeeruddin, S.M., Grätzel, M., 2017. Perovskite solar cells with CuSCN hole extraction layers yield stabilized efficiencies greater than 20%. Science (80-.). https://doi.org/10.1126/science.aam5655

Azri, F., Meftah, Afak, Sengouga, N., Meftah, Amjad, 2019. Electron and hole transport layers optimization by numerical simulation of a perovskite solar cell. Sol. Energy. https://doi.org/10.1016/j.solener.2019.02.017

Behrouznejad, F., Shahbazi, S., Taghavinia, N., Wu, H.P., Wei-Guang Diau, E., 2016. A study on utilizing different metals as the back contact of CH3NH3PbI3 perovskite solar cells. J. Mater. Chem. A. https://doi.org/10.1039/c6ta05938d

Brandt, R.E., Kurchin, R.C., Hoye, R.L.Z., Poindexter, J.R., Wilson, M.W.B., Sulekar, S., Lenahan, F., Yen, P.X.T., Stevanović, V., Nino, J.C., Bawendi, M.G., Buonassisi, T., 2015a. Investigation of Bismuth Triiodide (BiI3) for Photovoltaic Applications. J. Phys. Chem. Lett. https://doi.org/10.1021/acs.jpclett.5b02022

Brandt, R.E., Stevanović, V., Ginley, D.S., Buonassisi, T., 2015b. Identifying defect-tolerant semiconductors with high minority-carrier lifetimes: Beyond hybrid lead halide perovskites. MRS Commun. https://doi.org/10.1557/mrc.2015.26

Burgelman, M., Nollet, P., Degrave, S., 2000. Modelling polycrystalline semiconductor solar cells. Thin Solid Films. https://doi.org/10.1016/S0040-6090(99)00825-1

Bush, K.A., Palmstrom, A.F., Yu, Z.J., Boccard, M., Cheacharoen, R., Mailoa, J.P., McMeekin, D.P., Hoye, R.L.Z., Bailie, C.D., Leijtens, T., Peters, I.M., Minichetti, M.C., Rolston, N., Prasanna, R., Sofia, S., Harwood, D., Ma, W., Moghadam, F., Snaith, H.J., Buonassisi, T., Holman, Z.C., Bent, S.F., McGehee, M.D., 2017. 23.6%-efficient monolithic perovskite/silicon tandem solar cells with improved stability. Nat. Energy. https://doi.org/10.1038/nenergy.2017.9

Callahan, A., Cote, D., Capobianco, G., Balicki, M., 2018. Experimental and Theoretical Optimization of BiI3 Selective-Contact Solar Cell Materials. Major Qualif. Proj. (All Years).

Caprioglio, P., Stolterfoht, M., Wolff, C.M., Unold, T., Rech, B., Albrecht, S., Neher, D., 2019. On the Relation between the Open-Circuit Voltage and Quasi-Fermi Level Splitting in Efficient Perovskite Solar Cells. Adv. Energy Mater. https://doi.org/10.1002/aenm.201901631

Chakraborty, K., Choudhury, M.G., Paul, S., 2019. Numerical study of Cs2TiX6 (X = Br−, I−, F− and Cl−) based perovskite solar cell using SCAPS-1D device simulation. Sol. Energy. https://doi.org/10.1016/j.solener.2019.11.005

Chen, J., Zuo, L., Zhang, Y., Lian, X., Fu, W., Yan, J., Li, J., Wu, G., Li, C.Z., Chen, H., 2018. High-Performance Thickness Insensitive Perovskite Solar Cells with Enhanced Moisture Stability. Adv. Energy Mater. https://doi.org/10.1002/aenm.201800438

Chen, Z., Dong, Q., Liu, Y., Bao, C., Fang, Y., Lin, Y., Tang, S., Wang, Q., Xiao, X., Bai, Y., Deng, Y., Huang, J., 2017. Thin single crystal perovskite solar cells to harvest below-bandgap light absorption. Nat. Commun. https://doi.org/10.1038/s41467-017-02039-5

Cho, A.N., Park, N.G., 2017. Impact of Interfacial Layers in Perovskite Solar Cells. ChemSusChem. https://doi.org/10.1002/cssc.201701095

Cho, K.T., Paek, S., Grancini, G., Roldán-Carmona, C., Gao, P., Lee, Y., Nazeeruddin, M.K., 2017. Highly efficient perovskite solar cells with a compositionally engineered perovskite/hole transporting material interface. Energy Environ. Sci. https://doi.org/10.1039/c6ee03182j

Correa Baena, J.P., Steier, L., Tress, W., Saliba, M., Neutzner, S., Matsui, T., Giordano, F., Jacobsson, T.J., Srimath Kandada, A.R., Zakeeruddin, S.M., Petrozza, A., Abate, A., Nazeeruddin, M.K., Grätzel, M., Hagfeldt, A., 2015. Highly efficient planar perovskite solar cells through band alignment engineering. Energy Environ. Sci. https://doi.org/10.1039/c5ee02608c

Coulibaly, A.B., Oyedele, S.O., Kre, N.R., Aka, B., 2019. Comparative Study of Lead-Free Perovskite Solar Cells Using Different Hole Transporter Materials. Model. Numer. Simul.

Mater. Sci. https://doi.org/10.4236/mnsms.2019.94006

Coutinho, N.F., Cucatti, S., Merlo, R.B., Silva Filho, J.M.C., Villegas, N.F.B., Alvarez, F., Nogueira, A.F., Marques, F.C., 2019. The Thermomechanical Properties of Thermally Evaporated Bismuth Triiodide Thin Films. Sci. Rep. https://doi.org/10.1038/s41598-019-48194-1

Devi, C., Mehra, R., 2019. Device simulation of lead-free MASnI3 solar cell with CuSbS2 (copper antimony sulfide). J. Mater. Sci. https://doi.org/10.1007/s10853-018-03265-y

Domanski, K., Correa-Baena, J.P., Mine, N., Nazeeruddin, M.K., Abate, A., Saliba, M., Tress, W., Hagfeldt, A., Grätzel, M., 2016. Not All That Glitters Is Gold: Metal-Migration-Induced Degradation in Perovskite Solar Cells. ACS Nano. https://doi.org/10.1021/acsnano.6b02613

Duan, J., Xiong, Q., Feng, B., Xu, Y., Zhang, J., Wang, H., 2017. Low-temperature processed SnO 2 compact layer for efficient mesostructure perovskite solar cells. Appl. Surf. Sci. https://doi.org/10.1016/j.apsusc.2016.06.187

Elseman, A.M., Selim, M.S., Luo, L., Xu, C.Y., Wang, G., Jiang, Y., Liu, D.B., Liao, L.P., Hao, Z., Song, Q.L., 2019. Efficient and Stable Planar n-i-p Perovskite Solar Cells with Negligible Hysteresis through Solution-Processed Cu2O Nanocubes as a Low-Cost Hole-Transport Material. ChemSusChem. https://doi.org/10.1002/cssc.201901430

Eperon, G.E., Leijtens, T., Bush, K.A., Prasanna, R., Green, T., Wang, J.T.W., McMeekin, D.P., Volonakis, G., Milot, R.L., May, R., Palmstrom, A., Slotcavage, D.J., Belisle, R.A., Patel, J.B., Parrott, E.S., Sutton, R.J., Ma, W., Moghadam, F., Conings, B., Babayigit, A., Boyen, H.G., Bent, S., Giustino, F., Herz, L.M., Johnston, M.B., McGehee, M.D., Snaith, H.J., 2016. Perovskite-perovskite tandem photovoltaics with optimized band gaps. Science (80-.). https://doi.org/10.1126/science.aaf9717

Forgács, D., Gil-Escrig, L., Pérez-Del-Rey, D., Momblona, C., Werner, J., Niesen, B., Ballif, C., Sessolo, M., Bolink, H.J., 2017. Efficient Monolithic Perovskite/Perovskite Tandem Solar Cells. Adv. Energy Mater. https://doi.org/10.1002/aenm.201602121

Fu, L., Nie, Y., Li, B., Li, N., Cao, B., Yin, L., 2019. Bismuth Telluride Interlayer for All-Inorganic Perovskite Solar Cells with Enhanced Efficiency and Stability. Sol. RRL. https://doi.org/10.1002/solr.201900233

Gharibzadeh, S., Abdollahi Nejand, B., Jakoby, M., Abzieher, T., Hauschild, D., Moghadamzadeh, S., Schwenzer, J.A., Brenner, P., Schmager, R., Haghighirad, A.A., Weinhardt, L., Lemmer, U., Richards, B.S., Howard, I.A., Paetzold, U.W., 2019. Record Open-Circuit Voltage Wide-Bandgap Perovskite Solar Cells Utilizing 2D/3D Perovskite Heterostructure. Adv. Energy Mater. https://doi.org/10.1002/aenm.201803699

Gheno, A., Vedraine, S., Ratier, B., Bouclé, J., 2016. π-Conjugated materials as the hole-transporting layer in perovskite solar cells. Metals (Basel). https://doi.org/10.3390/met6010021

Gil-Escrig, L., Longo, G., Pertegás, A., Roldán-Carmona, C., Soriano, A., Sessolo, M., Bolink, H.J., 2015. Efficient photovoltaic and electroluminescent perovskite devices. Chem. Commun. https://doi.org/10.1039/c4cc07518h

Groeneveld, B.G.H.M., Adjokatse, S., Nazarenko, O., Fang, H.H., Blake, G.R., Portale, G., Duim, H., ten Brink, G.H., Kovalenko, M. V., Loi, M.A., 2020. Stable Cesium Formamidinium Lead Halide Perovskites: A Comparison of Photophysics and Phase Purity in Thin Films and Single Crystals. Energy Technol. https://doi.org/10.1002/ente.201901041

Hamdeh, U.H., Nelson, R.D., Ryan, B.J., Bhattacharjee, U., Petrich, J.W., Panthani, M.G., 2016. Solution-processed BiI3 thin films for photovoltaic applications: Improved carrier collection via solvent annealing. Chem. Mater. https://doi.org/10.1021/acs.chemmater.6b02347

Han, H., Hong, M., Gokhale, S.S., Sinnott, S.B., Jordan, K., Baciak, J.E., Nino, J.C., 2014. Defect engineering of BiI3 single crystals: Enhanced electrical and radiation performance for room temperature gamma-ray detection. J. Phys. Chem. C. https://doi.org/10.1021/jp411201k

Hu, Y., Zhang, S., Ruan, W., Wang, D., Wu, Y., Xu, F., 2020. Interfacing pristine BiI3 onto TiO2 for efficient and stable planar perovskite solar cells. Appl. Surf. Sci. https://doi.org/10.1016/j.apsusc.2019.144769

Igbari, F., Li, M., Hu, Y., Wang, Z.K., Liao, L.S., 2015. A room-temperature CuAlO2 hole interfacial layer for efficient and stable planar perovskite solar cells. J. Mater. Chem. A. https://doi.org/10.1039/c5ta07957h

Jiang, Q., Zhang, X., You, J., 2018. SnO2: A Wonderful Electron Transport Layer for Perovskite Solar Cells. Small. https://doi.org/10.1002/smll.201801154

Jung, M., Kim, Y.C., Jeon, N.J., Yang, W.S., Seo, J., Noh, J.H., Il Seok, S., 2016. Thermal Stability of CuSCN Hole Conductor-Based Perovskite Solar Cells. ChemSusChem. https://doi.org/10.1002/cssc.201600957

Karthick, S., Velumani, S., Bouclé, J., 2020. Experimental and SCAPS simulated formamidinium perovskite solar cells: A comparison of device performance. Sol. Energy. https://doi.org/10.1016/j.solener.2020.05.041

Kato, Y., Ono, L.K., Lee, M. V., Wang, S., Raga, S.R., Qi, Y., 2015. Silver Iodide Formation in Methyl Ammonium Lead Iodide Perovskite Solar Cells with Silver Top Electrodes. Adv. Mater. Interfaces. https://doi.org/10.1002/admi.201500195

Kim, G.W., Shinde, D. V., Park, T., 2015. Thickness of the hole transport layer in perovskite solar cells: Performance versus reproducibility. RSC Adv. https://doi.org/10.1039/c5ra18648j

Köhnen, E., Jošt, M., Morales-Vilches, A.B., Tockhorn, P., Al-Ashouri, A., Macco, B., Kegelmann, L., Korte, L., Rech, B., Schlatmann, R., Stannowski, B., Albrecht, S., 2019. Highly efficient monolithic perovskite silicon tandem solar cells: Analyzing the influence of current mismatch on device performance. Sustain. Energy Fuels. https://doi.org/10.1039/c9se00120d

Lang, F., Jošt, M., Frohna, K., Köhnen, E., Al-Ashouri, A., Bowman, A.R., Bertram, T., Morales-Vilches, A.B., Koushik, D., Tennyson, E.M., Galkowski, K., Landi, G., Creatore, M., Stannowski, B., Kaufmann, C.A., Bundesmann, J., Rappich, J., Rech, B., Denker, A., Albrecht, S., Neitzert, H.-C., Nickel, N.H., Stranks, S.D., 2020. Proton Radiation Hardness

of Perovskite Tandem Photovoltaics. Joule. https://doi.org/10.1016/j.joule.2020.03.006

Lee, J.W., Seol, D.J., Cho, A.N., Park, N.G., 2014. High-efficiency perovskite solar cells based on the black polymorph of HC(NH2)2PbI3. Adv. Mater. https://doi.org/10.1002/adma.201401137

Lee, L.C., Huq, T.N., Macmanus-Driscoll, J.L., Hoye, R.L.Z., 2018. Research Update: Bismuth-based perovskite-inspired photovoltaic materials. APL Mater. https://doi.org/10.1063/1.5029484

Lei, L., Zhang, S., Yang, S., Li, X., Yu, Y., Wei, Q., Ni, Z., Li, M., 2018. Influence of hole transport material/metal contact interface on perovskite solar cells. Nanotechnology. https://doi.org/10.1088/1361-6528/aab795

Li, F., Xu, M., Ma, X., Shen, L., Zhu, L., Weng, Y., Yue, G., Tan, F., Chen, C., 2018. UV Treatment of Low-Temperature Processed SnO2 Electron Transport Layers for Planar Perovskite Solar Cells. Nanoscale Res. Lett. https://doi.org/10.1186/s11671-018-2633-z

Lin, L., Jiang, L., Li, P., Fan, B., Qiu, Y., 2019. A modeled perovskite solar cell structure with a Cu2O hole-transporting layer enabling over 20% efficiency by low-cost low-temperature processing. J. Phys. Chem. Solids. https://doi.org/10.1016/j.jpcs.2018.09.024

Lin, L., Jiang, L., Li, P., Xiong, H., Kang, Z., Fan, B., Qiu, Y., 2020. Simulated development and optimized performance of CsPbI3 based all-inorganic perovskite solar cells. Sol. Energy. https://doi.org/10.1016/j.solener.2020.01.081

Liu, D., Wang, Y., Xu, H., Zheng, H., Zhang, T., Zhang, P., Wang, F., Wu, J., Wang, Z., Chen, Z., Li, S., 2019. SnO 2 -Based Perovskite Solar Cells: Configuration Design and Performance Improvement . Sol. RRL. https://doi.org/10.1002/solr.201800292

Liu, Y., Akin, S., Pan, L., Uchida, R., Arora, N., Milić, J. V., Hinderhofer, A., Schreiber, F., Uhl, A.R., Zakeeruddin, S.M., Hagfeldt, A., Ibrahim Dar, M., Grätzel, M., 2019. Ultrahydrophobic 3D/2D fluoroarene bilayer-based water-resistant perovskite solar cells with efficiencies exceeding 22%. Sci. Adv. https://doi.org/10.1126/sciadv.aaw2543

Lu, H., Liu, Y., Ahlawat, P., Mishra, A., Tress, W.R., Eickemeyer, F.T., Yang, Y., Fu, F., Wang, Z., Avalos, C.E., Carlsen, B.I., Agarwalla, A., Zhang, X., Li, X., Zhan, Y., Zakeeruddin, S.M., Emsley, L., Rothlisberger, U., Zheng, L., Hagfeldt, A., Grätzel, M., 2020. Vapor-assisted deposition of highly efficient, stable black-phase FAPbI3 perovskite solar cells. Science. https://doi.org/10.1126/science.abb8985

Marinova, N., Tress, W., Humphry-Baker, R., Dar, M.I., Bojinov, V., Zakeeruddin, S.M., Nazeeruddin, M.K., Grätzel, M., 2015. Light harvesting and charge recombination in CH3NH3PbI3 perovskite solar cells studied by hole transport layer thickness variation. ACS Nano. https://doi.org/10.1021/acsnano.5b00447

McMeekin, D.P., Sadoughi, G., Rehman, W., Eperon, G.E., Saliba, M., Hörantner, M.T., Haghighirad, A., Sakai, N., Korte, L., Rech, B., Johnston, M.B., Herz, L.M., Snaith, H.J., 2016. A mixed-cation lead mixed-halide perovskite absorber for tandem solar cells. Science (80-.). https://doi.org/10.1126/science.aad5845

McMeekin, D.P., Wang, Z., Rehman, W., Pulvirenti, F., Patel, J.B., Noel, N.K., Johnston, M.B.,

Marder, S.R., Herz, L.M., Snaith, H.J., 2017. Crystallization Kinetics and Morphology Control of Formamidinium–Cesium Mixed-Cation Lead Mixed-Halide Perovskite via Tunability of the Colloidal Precursor Solution. Adv. Mater. https://doi.org/10.1002/adma.201607039

Minemoto, T., Murata, M., 2015. Theoretical analysis on effect of band offsets in perovskite solar cells. Sol. Energy Mater. Sol. Cells. https://doi.org/10.1016/j.solmat.2014.10.036

Minemoto, T., Murata, M., 2014. Impact of work function of back contact of perovskite solar cells without hole transport material analyzed by device simulation. Curr. Appl. Phys. https://doi.org/10.1016/j.cap.2014.08.002

Ming, W., Yang, D., Li, T., Zhang, L., Du, M.H., 2018. Formation and Diffusion of Metal Impurities in Perovskite Solar Cell Material CH3NH3PbI3: Implications on Solar Cell Degradation and Choice of Electrode. Adv. Sci. https://doi.org/10.1002/advs.201700662

National Minerals Information Center, U., n.d. mcs2020.pdf - Mineral Commodity Summaries 2020.

Nazarenko, O., Yakunin, S., Morad, V., Cherniukh, I., Kovalenko, M. V., 2017. Single crystals of caesium formamidinium lead halide perovskites: Solution growth and gamma dosimetry. NPG Asia Mater. https://doi.org/10.1038/am.2017.45

Noel, N.K., Abate, A., Stranks, S.D., Parrott, E.S., Burlakov, V.M., Goriely, A., Snaith, H.J., 2014. Enhanced photoluminescence and solar cell performance via Lewis base passivation of organic-inorganic lead halide perovskites. ACS Nano. https://doi.org/10.1021/nn5036476

Nolan, M., 2008. Defects in Cu2O, CuAlO2 and SrCu2O2 transparent conducting oxides. Thin Solid Films. https://doi.org/10.1016/j.tsf.2008.04.020

NREL, 2020. Best Research-Cell Efficiency Chart | Photovoltaic Research | NREL 2020.

Prathapani, S., Bhargava, P., Mallick, S., 2018. Electronic band structure and carrier concentration of formamidinium-cesium mixed cation lead mixed halide hybrid perovskites. Appl. Phys. Lett. https://doi.org/10.1063/1.5016829

Qiu, L., He, S., Ono, L.K., Liu, S., Qi, Y., 2019. Scalable Fabrication of Metal Halide Perovskite Solar Cells and Modules. ACS Energy Lett. https://doi.org/10.1021/acsenergylett.9b01396

Rehman, W., McMeekin, D.P., Patel, J.B., Milot, R.L., Johnston, M.B., Snaith, H.J., Herz, L.M., 2017. Photovoltaic mixed-cation lead mixed-halide perovskites: Links between crystallinity, photo-stability and electronic properties. Energy Environ. Sci. https://doi.org/10.1039/c6ee03014a

Sahu, A., Dixit, A., 2018. Inverted structure perovskite solar cells: A theoretical study. Curr. Appl. Phys. https://doi.org/10.1016/j.cap.2018.10.008

Sanehira, E.M., Tremolet De Villers, B.J., Schulz, P., Reese, M.O., Ferrere, S., Zhu, K., Lin, L.Y., Berry, J.J., Luther, J.M., 2016. Influence of Electrode Interfaces on the Stability of Perovskite Solar Cells: Reduced Degradation Using MoOx/Al for Hole Collection. ACS Energy Lett. https://doi.org/10.1021/acsenergylett.6b00013

Shao, S., Loi, M.A., 2020. The Role of the Interfaces in Perovskite Solar Cells. Adv. Mater.

Interfaces. https://doi.org/10.1002/admi.201901469

Shasti, M., Mortezaali, A., 2019. Numerical Study of Cu2O, SrCu2O2, and CuAlO2 as Hole-Transport Materials for Application in Perovskite Solar Cells. Phys. Status Solidi Appl. Mater. Sci. https://doi.org/10.1002/pssa.201900337

Song, D., Wei, D., Cui, P., Li, M., Duan, Z., Wang, T., Ji, J., Li, Yaoyao, Mbengue, J.M., Li, Yingfeng, He, Y., Trevor, M., Park, N.G., 2016. Dual function interfacial layer for highly efficient and stable lead halide perovskite solar cells. J. Mater. Chem. A. https://doi.org/10.1039/c6ta00577b

Sutter-Fella, C.M., Ngo, Q.P., Cefarin, N., Gardner, K.L., Tamura, N., Stan, C. V., Drisdell, W.S., Javey, A., Toma, F.M., Sharp, I.D., 2018. Cation-Dependent Light-Induced Halide Demixing in Hybrid Organic-Inorganic Perovskites. Nano Lett. https://doi.org/10.1021/acs.nanolett.8b00541

Svanström, S., Jacobsson, T.J., Boschloo, G., Johansson, E.M.J., Rensmo, H., Cappel, U.B., 2020. Degradation Mechanism of Silver Metal Deposited on Lead Halide Perovskites. ACS Appl. Mater. Interfaces. https://doi.org/10.1021/acsami.9b20315

Wu, S., Chen, R., Zhang, S., Babu, B.H., Yue, Y., Zhu, H., Yang, Z., Chen, C., Chen, Weitao, Huang, Y., Fang, S., Liu, T., Han, L., Chen, Wei, 2019. A chemically inert bismuth interlayer enhances long-term stability of inverted perovskite solar cells. Nat. Commun. https://doi.org/10.1038/s41467-019-09167-0

Wu, Z., Liu, Z., Hu, Z., Hawash, Z., Qiu, L., Jiang, Y., Ono, L.K., Qi, Y., 2019. Highly Efficient and Stable Perovskite Solar Cells via Modification of Energy Levels at the Perovskite/Carbon Electrode Interface. Adv. Mater. https://doi.org/10.1002/adma.201804284

Xiong, L., Guo, Y., Wen, J., Liu, H., Yang, G., Qin, P., Fang, G., 2018. Review on the Application of SnO2 in Perovskite Solar Cells. Adv. Funct. Mater. https://doi.org/10.1002/adfm.201802757

Yoo, B., Ding, D., Marin-Beloqui, J.M., Lanzetta, L., Bu, X., Rath, T., Haque, S.A., 2019. Improved Charge Separation and Photovoltaic Performance of BiI3 Absorber Layers by Use of an in Situ Formed BiSI Interlayer. ACS Appl. Energy Mater. https://doi.org/10.1021/acsaem.9b00838

Yu, Y., Wang, C., Grice, C.R., Shrestha, N., Chen, J., Zhao, D., Liao, W., Cimaroli, A.J., Roland, P.J., Ellingson, R.J., Yan, Y., 2016. Improving the Performance of Formamidinium and Cesium Lead Triiodide Perovskite Solar Cells using Lead Thiocyanate Additives. ChemSusChem. https://doi.org/10.1002/cssc.201601027

Yuan, Z., Yang, Y., Wu, Z., Bai, S., Xu, W., Song, T., Gao, X., Gao, F., Sun, B., 2016. Approximately 800-nm-Thick Pinhole-Free Perovskite Films via Facile Solvent Retarding Process for Efficient Planar Solar Cells. ACS Appl. Mater. Interfaces. https://doi.org/10.1021/acsami.6b12637

Zhao, J., Zheng, X., Deng, Y., Li, T., Shao, Y., Gruverman, A., Shield, J., Huang, J., 2016. Is Cu a stable electrode material in hybrid perovskite solar cells for a 30-year lifetime? Energy

Environ. Sci. https://doi.org/10.1039/c6ee02980a

Zheng, J., Lau, C.F.J., Mehrvarz, H., Ma, F.J., Jiang, Y., Deng, X., Soeriyadi, A., Kim, J., Zhang, M., Hu, L., Cui, X., Lee, D.S., Bing, J., Cho, Y., Chen, C., Green, M.A., Huang, S., Ho-Baillie, A.W.Y., 2018. Large area efficient interface layer free monolithic perovskite/homo-junction-silicon tandem solar cell with over 20% efficiency. Energy Environ. Sci. https://doi.org/10.1039/c8ee00689j

Zheng, X., Chen, H., Li, Q., Yang, Y., Wei, Z., Bai, Y., Qiu, Y., Zhou, D., Wong, K.S., Yang, S., 2017. Boron Doping of Multiwalled Carbon Nanotubes Significantly Enhances Hole Extraction in Carbon-Based Perovskite Solar Cells. Nano Lett. https://doi.org/10.1021/acs.nanolett.7b00200